NeuroImage: Clinical 24 (2019) 102006

Contents lists available at ScienceDirect

NeuroImage: Clinical

journal homepage: www.elsevier.com/locate/ynicl

Altered white matter structure in auditory tracts following early monocular enucleation

Nikita A. Wong[a,b], Sara A. Rafique[a,b], Stefania S. Moro[a,b,d], Krista R. Kelly[c], Jennifer K.E. Steeves[a,b,d,*]

[a] Department of Psychology, York University, Toronto, ON, Canada
[b] Centre for Vision Research, York University, Toronto, ON, Canada
[c] Retina Foundation of the Southwest, Dallas, TX, USA
[d] Department of Ophthalmology and Visual Sciences, The Hospital for Sick Children, Toronto, ON, Canada

ARTICLE INFO

Keywords:
Development
Vision
Magnetic resonance imaging
Diffusion tensor imaging
Monocular enucleation
Multisensory
Morphology

ABSTRACT

Purpose: Similar to early blindness, monocular enucleation (the removal of one eye) early in life results in crossmodal behavioral and morphological adaptations. Previously it has been shown that partial visual deprivation from early monocular enucleation results in structural white matter changes throughout the visual system (Wong et al., 2018). The current study investigated structural white matter of the auditory system in adults who have undergone early monocular enucleation compared to binocular control participants. Methods: We reconstructed four auditory and audiovisual tracts of interest using probabilistic tractography and compared microstructural properties of these tracts to binocularly intact controls using standard diffusion indices. Results: Although both groups demonstrated asymmetries in indices in intrahemispheric tracts, monocular enucleation participants showed asymmetries opposite to control participants in the auditory and A1-V1 tracts. Monocular enucleation participants also demonstrated significantly lower fractional anisotropy in the audiovisual projections contralateral to the enucleated eye relative to control participants. Conclusions: Partial vision loss from early monocular enucleation results in altered structural connectivity that extends into the auditory system, beyond tracts primarily dedicated to vision.

1. Introduction

Visual deprivation during early postnatal development results in changes to remaining intact sensory systems to accommodate for the loss of vision (Merabet and Pascual-Leone, 2010). There is an extensive body of research supporting crossmodal behavioral adaptations (e.g., faster language processing (Röder et al., 2002)), and functional recruitment of visual cortex for nonvisual tasks (e.g., sound localization (Weeks et al., 2000)) following early blindness. Early monocular enucleation, the surgical removal of one eye, is a unique model for examining the consequences of the loss of binocularity (for review: Steeves et al., 2008). Unlike other forms of monocular visual deprivation, such as cataract or strabismus, that result in anomalous binocular visual input, surgically removing the eye completely eliminates all visual input to the brain from that eye (Steeves et al., 2008).

Monocular enucleation has been shown to result in crossmodal behavioral and morphological adaptations similar to those seen following early blindness. Assessment of binaural sound localization has revealed that monocular enucleation participants (compared to controls viewing binocularly, monocularly, and with their eyes shut) have significantly greater accuracy in the central region of space (i.e., within 78° to the left or right of straight ahead) and less bias toward localizing sounds as 'straight ahead' (Hoover et al., 2012). Moreover, participants who have undergone early monocular enucleation do not show the typical visual dominance demonstrated by controls (i.e., the Colavita visual dominance effect: Moro and Steeves, 2012; Moro and Steeves, 2013). Rather, they appear to weight auditory and visual stimuli equally, and continue to do so when the temporal load for the task is increased (Moro and Steeves, 2012; Moro and Steeves, 2013). Participants who have undergone early monocular enucleation also show comparable spatial and temporal audiovisual localization abilities to those of control participants. Thus, despite taking significantly longer to localize unimodal visual stimuli compared to unimodal auditory stimuli, they demonstrate optimal audiovisual integration relative to controls (Moro et al., 2014).

Recently, using diffusion tensor imaging (DTI), we have shown that

* Corresponding author at: 1032 Sherman Health Science Research Centre, York University, 4700 Keele St., Toronto, ON M3J 1P3, Canada.
E-mail address: steeves@yorku.ca (J.K.E. Steeves).

https://doi.org/10.1016/j.nicl.2019.102006
Received 2 May 2019; Received in revised form 4 September 2019; Accepted 14 September 2019
Available online 16 September 2019

early monocular enucleation results in structural white matter changes throughout the visual system (Wong et al., 2018). Using standard DTI indices and probabilistic tractography, we observed asymmetries in the monocular enucleation group that were opposite to those observed in controls for fractional anisotropy (FA), mean diffusivity (MD), and radial diffusivity (RD) in the optic radiations, the projections from primary visual cortex (V1) to the lateral geniculate nucleus (LGN), and the interhemispheric V1 projections (Wong et al., 2018). Early monocular enucleation was associated with significantly lower FA bidirectionally in the interhemispheric V1 projections (Wong et al., 2018). These differences were consistently greater for the tracts contralateral to the enucleated eye and are consistent with the asymmetric LGN volumes and optic tract diameters previously observed in this group of participants (Kelly et al., 2014). Likewise, the changes observed in the interhemispheric V1 projections (Wong et al., 2018) are consistent with the significantly larger surface area and gyrification of ipsilateral V1 of monocular enucleation participants (Kelly et al., 2015). These differences in structural connectivity may be related to changes in visual processing reported following early monocular enucleation (e.g., impaired motion processing; for review: Kelly et al., 2012; Steeves et al., 2008).

Findings from studies in early blind participants indicate that white matter changes also occur outside of the visual system, including structures connecting frontal and temporal regions, frontal and somatosensory regions, and the corticospinal tracts (Yu et al., 2007). Long-term structural changes in the auditory and multisensory systems have been observed following early monocular enucleation. A hemispheric asymmetry in the medial geniculate body (MGB), the auditory nucleus of the thalamus, is present in only monocular enucleation participants, where the left MGB volume is significantly larger than the right MGB, independent of eye of enucleation (Moro et al., 2014). Additionally, increased gray matter surface area and gyrification in cortical regions responsible for auditory and multisensory processing have been demonstrated following early monocular enucleation (Kelly et al., 2015). Given that the previously reported white matter differences within the visual system are consistent with gray matter differences (Kelly et al., 2014; Kelly et al., 2015; Wong et al., 2018), and that gray matter differences are also found in auditory and multisensory regions (Kelly et al., 2015), it is possible that white matter structures connecting auditory and audiovisual regions are also altered following early monocular enucleation.

In the present study, we extend our previous findings of altered white matter in the visual system to examine the potential long-term consequences of early monocular enucleation on white matter tracts associated with auditory and audiovisual processing. Given the cross-modal changes previously observed in this group (Hoover et al., 2012), four auditory and audiovisual tracts of interest were targeted, including: 1) the auditory radiations (connecting the MGB to primary auditory cortex [A1]), 2) the projections from A1 to the MGB, 3) the A1-V1 projections (Beer et al., 2011; Beer et al., 2013),and 4) the projections from V1 to A1. Probabilistic tract reconstruction was performed and comparisons of DTI indices (fractional anisotropy [FA], axial diffusivity [AD], mean diffusivity [MD] and radial diffusivity [RD]) were made between participants who had undergone early monocular enucleation and binocularly intact controls.

2. Methods

2.1. Participants

2.1.1. Monocular enucleation participants (ME)

Seven adults (3 female; mean age ± SD = 27.3 ± 10.0 years; range = 16–43 years) who had undergone early monocular enucleation due to retinoblastoma, a childhood cancer of the retina, participated in this study. Unilateral eye-enucleation (3 right-eye) was performed at 24.0 ± 18.1 months of age (range = 4–60 months). All participants had normal or corrected-to-normal vision in their remaining eye (≥ 20/20; ETDRS chart, Precision Vision™, La Salle, IL). Individual patient histories are reported in Table 1.

Table 1
Patient histories for monocular enucleation participants.

Participant	Age (years)	Sex	Snellen acuity	Enucleated eye	AAE[a] (months)
ME01	28	Male	20/12.5	Right	4
ME02	30	Male	20/20 + 3	Left	13
ME03	43	Female	20/12.5 + 2	Right	18
ME04	17	Female	20/12.5 + 1	Right	26
ME05	36	Female	20/16 + 4	Left	18
ME06	21	Male	20/16	Left	60
ME07	16	Male	20/20 + 4	Left	32

[a] AAE = age at enucleation.

2.1.2. Binocularly intact control participants (BC)

Eleven age-matched controls (7 female; 27.8 ± 5.7 years; 18–40 years) participated in this study. All participants had normal or corrected-to-normal visual acuity (≥ 20/20; ETDRS chart) and normal stereoacuity (40 arcsec; Titmus test, Stereo Optical Co., Inc., Chicago, IL).

Both participant groups reported no known contraindications to MRI and had previously participated in our DTI study investigating visual white matter structures in this group (Wong et al., 2018). All participants provided written informed consent prior to their participation. This study was approved by the York University Office of Research Ethics and was conducted in accordance with the 1964 Declaration of Helsinki.

2.2. Data acquisition

All scans were acquired on a Siemens MAGNETOM® Tim Trio 3 T MRI scanner using a 32-channel head coil (Erlangen, Germany). Using a T1-weighted 3D magnetization-prepared rapid gradient-echo (MPRAGE) imaging sequence, high-resolution whole brain anatomical images were obtained sagittally with the following parameters: TR = 1900 ms, TE = 2.52 ms, 1 mm^3.

isotropic voxels, imaging matrix = 256 × 256, FOV = 256 mm, flip angle = 9°, and number of slices = 192. A diffusion-weighted echo-planar imaging sequence was used to obtain whole brain DTI data in 64 diffusion directions, including a single reference volume (b_0 = 0 s/mm^2), with the following parameters: TR = 6900 ms, TE = 86 ms, 1.5 × 1.5 × 2.0 mm voxels, imaging matrix = 128 × 128, FOV = 192 mm, parallel imaging (GRAPPA with acceleration factor of 3), b = 1000 s/mm^2, and number of contiguous slices = 56.

2.3. Data processing

Data acquisition and processing were performed in accordance with the procedures of Wong et al. (2018) using freely available tools from the FMRIB3's Software Library (FSL; version 5.0.8; http://www.fmrib.ox.ac.uk/fsl) (Smith et al., 2004). For a full overview of the data acquisition and processing procedures used in this study please see Wong et al. (2018).

2.3.1. Pre-processing

Non-brain tissue was removed from both the T1-weighted anatomical images and eddy current corrected diffusion-weighted images using FSL's Brain Extraction Tool (BET) (Smith, 2002). Linear registration of the anatomical images to the standard Montreal Neurological Institute (MNI) space template was then performed using FSL's Linear Registration Tool (FLIRT) (Jenkinson et al., 2002; Jenkinson and Smith, 2001). The brain-extracted diffusion-weighted images were likewise

Table 2
Value of diffusion indices ($\times 10^3$) of white matter tracts of interest.

White matter structure	Diffusion parameter	Binocular control group		Monocular enucleation group	
		Ipsi[a]	Contra[a]	Ipsi[b]	Contra[b]
MGB-A1	AD[c]	1.254 ± 0.049	1.181 ± 0.058	1.230 ± 0.048	1.202 ± 0.063
	FA	0.592 ± 0.025	0.589 ± 0.037	0.582 ± 0.045	0.569 ± 0.039
	MD[c]	0.723 ± 0.028	0.686 ± 0.027	0.715 ± 0.038	0.711 ± 0.045
	RD[c]	0.457 ± 0.029	0.439 ± 0.034	0.458 ± 0.048	0.465 ± 0.046
A1-MGB	AD[c]	1.178 ± 0.035	1.143 ± 0.047	1.187 ± 0.027	1.182 ± 0.063
	FA	0.546 ± 0.027	0.544 ± 0.035	0.541 ± 0.036	0.555 ± 0.064
	MD[c]	0.710 ± 0.025	0.692 ± 0.031	0.715 ± 0.024	0.708 ± 0.042
	RD[c]	0.476 ± 0.029	0.467 ± 0.036	0.479 ± 0.034	0.472 ± 0.057
A1-V1	AD[c]	1.253 ± 0.040	1.229 ± 0.041	1.248 ± 0.029	1.217 ± 0.052
	FA	0.550 ± 0.035	0.556 ± 0.031	0.529 ± 0.019	0.521 ± 0.021
	MD[c]	0.743 ± 0.031	0.728 ± 0.032	0.757 ± 0.025	0.745 ± 0.029
	RD[c]	0.488 ± 0.034	0.477 ± 0.037	0.511 ± 0.027	0.508 ± 0.024
V1-A1	AD[c]	1.256 ± 0.041	1.246 ± 0.052	1.247 ± 0.025	1.224 ± 0.059
	FA	0.546 ± 0.030	0.558 ± 0.029	0.525 ± 0.021	0.529 ± 0.019
	MD[c]	0.748 ± 0.029	0.734 ± 0.031	0.759 ± 0.025	0.744 ± 0.033
	RD[c]	0.494 ± 0.030	0.478 ± 0.035	0.514 ± 0.027	0.503 ± 0.024

Values of the diffusion indices measured for the binocular control and monocular enucleation group.
[a] Relative to the non-dominant eye.
[b] Relative to the enucleated eye.
[c] Values reported are $\times 10^{-3}\,mm^2/s$.

registered to the MNI space template, as well as, to the T1-weighted anatomical image using FSL's Non-Linear Registration Tool (FNIRT) (Andersson et al., 2007a, 2007b). DTIFIT from FSL's Diffusion Toolbox (FDT) was used to fit local diffusion tensor models using a standard linear regression approach at each voxel of the pre-processed diffusion data. In order to obtain the diffusion parameters necessary for probabilistic tract reconstruction, FSL's Bayesian Estimation of Diffusion Parameters Obtained using Sampling Techniques for modeling Crossing Fibers (BEDPOSTX) was run through FDT (Behrens et al., 2007; Behrens et al., 2003).

2.3.2. Probabilistic tractography

Using FSL's Probabilistic Tracking with Crossing Fibers (PROBTRACKX) tool, probabilistic tract reconstruction was performed for the auditory radiations (MGB-A1), A1-MGB projections, A1-V1 projections, and V1-A1 projections, in each hemisphere separately. The masks necessary to perform reconstruction were obtained from the Jülich Histological atlas (Eickhoff et al., 2005; Eickhoff et al., 2007) and Harvard-Oxford Subcortical Structural atlas (Frazier et al., 2005; Goldstein et al., 2007) available through FSL. Seed masks consisted of the MGB and A1 for the auditory radiations and A1-V1 tracts, respectively. Termination masks consisted of A1 and V1, which were also used as waypoint masks (identify only the tracts passing through the specified region), for the auditory radiations and A1-V1 projections. The reverse tractography was performed in order to investigate the connections from termination to seed masks (i.e., the MGB-A1 projections and V1-A1 projections). To reduce the number of false positive streamlines (tracts), an exclusion mask consisting of cerebral white matter of the opposite hemisphere was used for all reconstructions (Behrens et al., 2007; Behrens et al., 2003). PROBTRACKX was run under the same settings previously used to compare visual system white matter structure between binocularly intact controls and participants who had undergone early monocular enucleation (Wong et al., 2018). Reference to seed and termination points does not imply tract directionality (which cannot be inferred from probabilistic tractography), but only refers to tract start and end points.

2.3.3. Extraction of diffusion parameters

FSL's Tract-Based Spatial Statistics (TBSS) was used to extract the diffusion indices bilaterally from the four tracts of interest. Diffusion indices include; AD (Axial Diffusivity; degree of diffusion parallel to the axon), FA (Fractional Anisotropy; degree of directionality, or anisotropy, of a diffusion process), MD (Mean Diffusivity; average rate of diffusion within a voxel), and RD (Radial Diffusivity; degree of diffusion perpendicular to the axon). Each participant's MNI space diffusion-weighted data was used to create an individual mean FA map (or mean FA skeleton) at a threshold $FA > 0.2$. Affine nonlinear registration (FNIRT) was then used to align the data for the remaining diffusion indices before they were individually projected onto the mean skeleton. Values for all diffusion parameters were subsequently extracted from the auditory radiations, MGB-A1 projections, A1-V1 projections, and V1-A1 projections using masks of the PROBTRACKX generated tracts (Smith et al., 2006).

2.4. Statistical analysis

The open source program R (version 3.2.2; http://www.R-project.org) was used to perform all statistical analyses. Due to the non-normality of the data, independent and repeated-measures pairwise comparisons for the four tracts of interest were conducted using Yuen's test (T_y) with 10% trimmed means. Multiple comparisons were controlled for using the false-discovery rate (FDR).

3. Results

There was no significant effect of sex on the tracts of interest investigated, $p > .05$. Therefore, sex was not factored into the following analyses.

As in our previous investigation (Wong et al., 2018), all results are reported relative to the non-dominant eye in controls and the enucleated eye in monocular enucleation participants in order to standardize the hemispheric comparisons. Findings in controls will be referred to as ipsilateral or contralateral to the non-dominant eye, and results for monocular enucleation participants will be reported as ipsilateral or contralateral to the enucleated (i.e., non-dominant) eye. Eye dominance was assessed in the control participants using visual acuity and the Porta test (described in Durand and Gould, 1910). There is a growing literature base examining the variability of eye dominance in individuals with normal visual acuity (see Li et al., 2010). Findings have revealed that only a minority of the population demonstrates strong and consistent eye dominance. Given that the purpose of our study is not to use eye dominance as the basis for clinical decision-

making, nor to assess behavioral performance in control participants, even weak eye dominance is sufficient. Table 2 provides the values of the white matter variables described in the results section.

3.1. Tracts of interest

3.1.1. Auditory radiations (MGB-A1)

Within groups pairwise comparisons revealed asymmetries in AD, $T_y(17) = -11.179$, $p < .001$, FA, $T_y(17) = -6.746$, $p < .001$, and MD, $T_y(17) = -11.183$, $p < .001$, in controls such that significantly larger values were observed for the auditory radiation ipsilateral, compared to contralateral, to the non-dominant eye (Fig. 1). These asymmetries were also found in monocular enucleation participants with the auditory radiation ipsilateral to the enucleated eye having significantly higher AD, $T_y(11) = -9.204$, $p < .001$, FA, $T_y(11) = -5.585$, $p < .001$, and MD, $T_y(11) = -9.207$, $p < .001$. However, analysis of the RD data revealed opposite asymmetries across groups with larger values observed in the auditory radiation ipsilateral to the non-dominant eye in controls, $T_y(17) = -11.185$, $p < .001$, but higher RD in the auditory radiation contralateral to the enucleated eye in monocular enucleation participants, $T_y(11) = 9.209$, $p < .001$. Nevertheless, monocular enucleation participants did not differ significantly from controls across any of the measured diffusion parameters, $ps > .05$.

3.1.2. A1-MGB projections

Similar to the auditory radiations, controls demonstrated significantly higher values for AD, $T_y(17) = -11.180$, $p < .001$, FA, $T_y(17) = -7.068$, $p < .001$, MD, $T_y(17) = -11.183$, $p < .001$, and RD, $T_y(17) = -11.189$, $p < .001$, in the A1-MGB projections ipsilateral to the non-dominant eye. The same asymmetries in AD, $T_y(11) = -9.204$, $p < .001$, MD, $T_y(11) = -9.207$, $p < .001$, and RD, $T_y(11) = -9.212$, $p < .001$, were also present in monocular enucleation participants; however, in contrast to controls, significantly larger values for FA, $T_y(11) = 5.877$, $p < .001$, were observed in the A1-MGB projections contralateral, rather than ipsilateral, to the enucleated eye. There were no significant differences between groups for AD, FA, MD, or RD in the A1-MGB projections, $ps > .05$. Mean values for the A1-MGB projections for both groups are shown in Fig. 1.

3.1.3. A1-V1 projections

Within-group comparisons indicated that controls exhibited significantly higher AD, $T_y(17) = -11.179$, $p < .001$, MD, $T_y(17) = -11.183$, $p < .001$, and RD, $T_y(17) = -11.185$, $p < .001$, in the A1-V1 projections ipsilateral to the non-dominant eye, but larger FA, $T_y(17) = 7.112$, $p < .001$, in the A1-V1 projections contralateral to the non-dominant eye. In contrast, monocular enucleation participants had significantly higher FA, $T_y(11) = -5.969 = -5.969$, $p < .001$, in the A1-V1 projections ipsilateral to the enucleated eye, as well as, larger AD, $T_y(11) = -9.204$, $p < .001$, MD, $T_y(11) = -9.207$, $p < .001$, and RD, $T_y(11) = -9.209$, $p < .001$, values in the same hemisphere. Reconstruction of the projections connecting A1 to V1 revealed significantly lower FA in the contralateral tracts of monocular enucleation participants relative to the controls, $T_y(14) = 2.397$, $p = .042$ (Fig. 1).

3.1.4. V1-A1 projections

The same pattern of asymmetries as tracking from A1 to V1 was observed for the controls with the V1-A1 projections. V1-A1 projections ipsilateral to the non-dominant eye demonstrated significantly higher AD, $T_y(17) = -11.179$, $p < .001$, MD, $T_y(17) = -11.183$, $p < .001$, and RD, $T_y(17) = -11.185$, $p < .001$; and the contralateral V1-A1 projections demonstrated larger FA, $T_y(17) = 7.173$, $p < .001$. Monocular enucleation participants likewise showed these asymmetries with higher values for AD, $T_y(11) = -9.204$, $p < .001$, MD, $T_y(11) = -9.207$, $p < .001$, and RD, $T_y(11) = -9.209$, $p < .001$, in the tracts ipsilateral compared to contralateral to the enucleated eye, and with FA showing the opposite asymmetry, $T_y(11) = 6.002$, $p < .001$. Tracking of V1-A1 also revealed significantly lower FA, $T_y(14) = 1.290$, $p = .037$, in the projections contralateral to the removed eye in monocular enucleation participants compared to controls (Fig. 1).

4. Discussion

This study investigated whether changes in white matter structure occur in the auditory system in adults who had undergone early monocular enucleation. We reconstructed four auditory and audiovisual tracts of interest using probabilistic tractography and examined these structures in individuals with early monocular enucleation compared to binocularly intact controls using standard diffusion indices (i.e., AD, FA, MD, RD). Similar to our observations in the white matter structures of the visual system (Wong et al., 2018), both groups demonstrated asymmetries in intrahemispheric tracts. Monocular enucleation participants, however, showed asymmetries opposite to control participants in the auditory and A1-V1 tracts. They also demonstrated significantly lower FA in the audiovisual projections contralateral to the enucleated eye only. Overall, these findings suggest that partial vision loss from early monocular enucleation results in alterations to structural connectivity that extend beyond tracts primarily dedicated to vision and into tracts involved in auditory processing.

The auditory radiations were of particular interest due to the larger MGB volume (Moro et al., 2015) and increased surface area and gyrification previously observed in higher-level auditory cortex (Kelly et al., 2015) in monocular enucleation participants. Control participants showed significantly larger AD, FA, MD, and RD values in the tracts ipsilateral to the non-dominant eye in both the auditory radiations and reconstructions from A1 to the MGB, suggesting an overall increase in the degree and directionality of diffusion in these tracts. It is surprising that control participants would demonstrate eye-dominance dependent asymmetries in these auditory tracts given that most known auditory asymmetries are due to hemisphere localization (Hutsler and Galuske, 2003; Zatorre et al., 2002). There is increasing evidence, however, that while primary sensory regions chiefly process information for that sense, they are also, to a degree, multimodal (Driver and Noesselt, 2008; Martuzzi et al., 2007; Schroeder and Foxe, 2005). For example, visual stimuli can activate auditory cortex in control participants (Meyer et al., 2010; Pekkola et al., 2005). Therefore, it is possible that asymmetries in the visual system (Wong et al., 2018) may be reflected in the auditory system. Inferences drawn from these findings are limited due to the fact that ear dominance was not controlled for in this study (Zatorre, 1989).

Participants who had undergone monocular enucleation had significantly larger RD in the auditory radiation contralateral to the removed eye, whereas controls demonstrated the opposite asymmetry (relative to their non-dominant eye). Higher RD in the hemisphere contralateral to the enucleated eye could indicate a number of changes following early monocular enucleation (Boucard et al., 2016; Jones et al., 2013). For example, larger RD values can reflect greater fiber caliber (Jones et al., 2013; Schmierer et al., 2007; Song et al., 2002; Song et al., 2005), which may indicate an attempt to increase the available information flow in that hemisphere. Increased RD can also indicate disorganization due to the growth of new axons (Jones et al., 2013; O'Brien and Olavarria, 1994; Olavarria and Malach, 1987). Growth of new axons may be a more likely explanation for the current results given that several higher order auditory regions (e.g., supramarginal areas) exhibit significantly increased surface area and/or gyrification in the hemisphere contralateral to the enucleated eye (Kelly et al., 2015). These structural increases may facilitate greater functional activation in A1, which in turn encourages the growth of new axons in that hemisphere to support the incoming information (Jones et al., 2013; Song et al., 2002; Song et al., 2005). Although changes in structure do not necessarily reflect differences in function, it is possible that this reversed RD asymmetry may contribute to the differences in

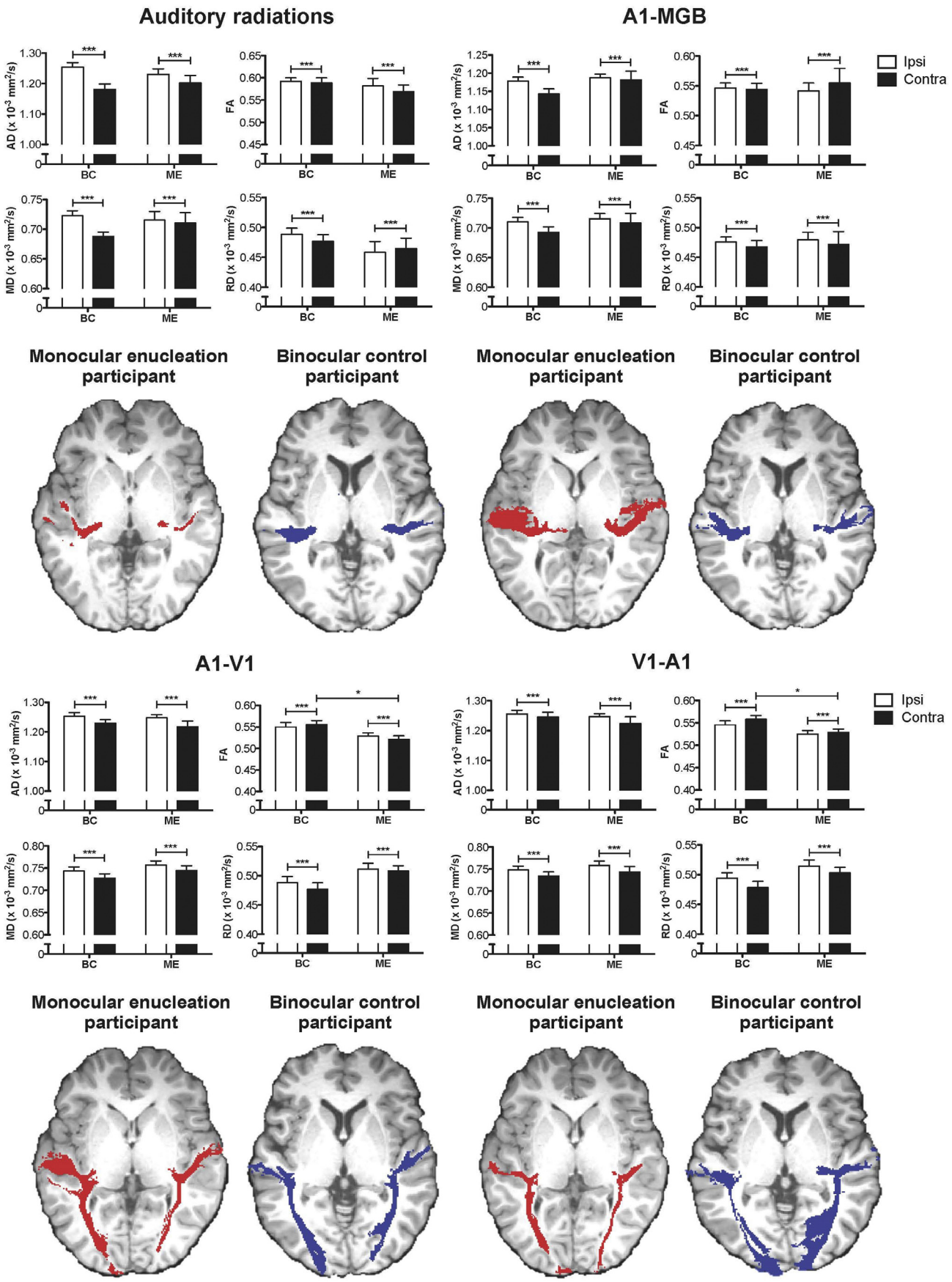

(caption on next page)

Fig. 1. Mean values of the diffusion parameters (AD [$\times 10^{-3}$ mm^2/s], FA, MD [$\times 10^{-3}$ mm^2/s], and RD [$\times 10^{-3}$ mm^2/s]) in the ipsilateral (to the enucleated or non-dominant eye) and contralateral tracts of interest for controls (BC) and monocular enucleation participants (ME). Error bars represent ± SEM. Examples of the probabilistic tractography reconstructions of the auditory radiations (MGB-A1 projections), A1-MGB projections, A1-V1 projections, and V1-A1 projections are shown under the associated graphs for a single control participant and monocular enucleation participant. AD = axial diffusivity; FA = fractional anisotropy; MD = mean diffusivity; RD = radial diffusivity. $^{*}p < .05$; $^{**}p < .01$; $^{***}p < .001$.

auditory behavior (e.g., localization) observed in this group (Hoover et al., 2012). Functional MRI (fMRI) data will be crucial to revealing any functional consequences of these structural changes.

The A1-MGB projections in monocular enucleation participants showed a reversed FA asymmetry relative to controls. In contrast to the auditory radiations, the A1-MGB projections contralateral to the enucleated eye demonstrate better coherence of fiber orientation and improved tract organization as indicated by greater FA (Jones et al., 2013; Jones, 2008) compared to the ipsilateral hemisphere. Improved tract organization in the A1-MGB projections may reflect an attempt to compensate for disorganization in the contralateral auditory radiations.

Both controls and monocular enucleation participants showed the same set of asymmetries in all but one diffusion parameter (FA) when the projections were tracked from A1 to V1 and V1 to A1. The visual pathway ipsilateral to the non-dominant eye benefits from greater physiological input or functional activity (incoming from the dominant eye) relative to the contralateral visual pathway (Menon et al., 1997; Miki et al., 2001; Rombouts et al., 1996; Toosy et al., 2001). This imbalance may be reflected in other tracts associated with the visual system. The higher values for AD, MD, and RD in the hemisphere ipsilateral to the non-dominant eye could indicate larger axon diameters or more abundant tracts (Jones et al., 2013; Jones, 2008; Le Bihan, 2003; Pierpaoli and Basser, 1996) to facilitate the larger amount of information. Yet, monocular enucleation participants demonstrate significantly lower FA in the A1-V1 projections contralateral to the enucleated eye, an asymmetry opposite to that of controls (relative to their non-dominant eye). This likely contributes to the significantly lower FA values relative to controls in the A1-V1 (as well as V1-A1) projections contralateral to the enucleated eye. Lower FA values indicate decreased coherence of fiber orientation, which is often broadly interpreted as tract disorganization (Jones et al., 2013; Jones, 2008). The significant reduction in FA in the contralateral projections connecting A1 and V1 compared to controls is consistent with the known morphological changes in the visual system following early monocular enucleation (Wong et al., 2018; Moro et al., 2015; Kelly et al., 2014). The optic tract and LGN are significantly smaller in the contralateral hemisphere compared to ipsilateral to the enucleated eye (Kelly et al., 2014). These asymmetries are reflected in the optic radiations, which show significantly lower FA in the hemisphere contralateral compared to ipsilateral to the enucleated eye (Wong et al., 2018). Thus, the reduced FA in the projections between A1 and V1 observed in this study could be an extension of changes in the visual system in the contralateral hemisphere, possibly through transneuronal degeneration. Changes in functional activity in V1 have the potential to impact other related structures, such as the projections between A1 and V1, and can result in axonal degeneration and immaturity, both of which have been previously associated with reduced FA following vision loss (Boucard, et al., 1989; Shu et al., 2009).

Lastly, it has been found that participants who have undergone monocular enucleation have significantly greater surface area and gyrification in V1 ipsilateral to the enucleated eye compared to controls (Kelly et al., 2015). This increased surface area and gyrification may support the absence of significant between-group differences in FA values in the A1-V1 and V1-A1 projections ipsilateral to the non-dominant eye of both groups despite the loss of one eye. Contralateral V1 does not demonstrate these structural increases, which may contribute to significantly lower FA in the contralateral hemisphere.

Results of the current study are limited by the sample size, as is typical when investigating patient groups with rare conditions. Efforts to compensate for the sample size included ensuring that each patient was approximately age and sex matched with the control group, and by employing non-parametric statistical analyses.

In conclusion, we report long-term changes in white matter structures in the auditory system in adults who have undergone early monocular enucleation. Monocular enucleation participants showed instances of asymmetries in standard diffusion indices in the auditory radiations, A1-MGB, and A1-V1 tracts, that were opposite to that of controls. The observed differences in the white matter structures in monocular enucleation participants may support the previously observed audiovisual behavioral (Hoover et al., 2012; Moro and Steeves, 2012; Moro and Steeves, 2013; Moro et al., 2014) and structural differences (Moro et al., 2015; Kelly et al., 2015). These results contribute to our understanding of the morphological adaptations underlying behavioral changes seen in participants who have undergone monocular enucleation (Kelly et al., 2014). These findings suggest that partial vision loss from early monocular enucleation results in alterations to structural connectivity that extend beyond tracts primarily dedicated to vision.

Declaration of Competing Interest

The authors have no conflicts of interest to declare.

Acknowledgements

We sincerely thank all participants for taking part in our research.

References

Andersson, J.L., Jenkinson, M., Smith, S., 2007a. Non-linear Optimisation. FMRIB Technical Report TR07JA1. University of Oxford FMRIB Centre, Oxford, UK.
Andersson, J.L., Jenkinson, M., Smith, S., 2007b. Non-linear Registration, Aka Spatial Normalisation. FMRIB Technical Report TR07JA2. University of Oxford FMRIB Centre, Oxford, UK.
Beer, A.L., Plank, T., Greenlee, M.W., 2011. Diffusion tensor imaging shows white matter tracts between human auditory and visual cortex. Exp. Brain Res. 299–308.
Beer, A.L., Plank, T., Meyer, G., Greenlee, M.W., 2013. Combined diffusion-weighted and functional magnetic resonance imaging reveals a temporal-occipital network involved in auditory-visual object processing. Front. Integr. Neurosci. 1–20.
Behrens, T.E.J., Woolrich, M.W., Jenkinson, M., Johansen-Berg, H., Nunes, R.G., Clare, S., Matthews, P.M., Brady, J.M., Smith, S.M., 2003. Characterization and propagation of uncertainty in diffusion-weighted MRimaging. Magn. Reson. Med. 50, 1077–1088.
Behrens, T.E.J., Johansen-Berg, H., Jbabdi, S., Rushworth, M.F.S., Woolrich, M.W., 2007. Probabilistic diffusion tractography with multiple fibre orientations: what can we gain? NeuroImage 34, 144–155.
Boucard, C.C., Hanekamp, S., ĆurčiĆ-Blake, B., Ida, M., Yoshida, M., Cornelissen, F.W., 2016. Neurodegeneration beyond the primary visual pathways in a population with a high incidence of normal-pressure glaucoma. Ophthalmic Physiol. Opt. 36, 344–353.
Driver, J., Noesselt, T., 2008. Multisensory interplay reveals crossmodal influences on 'sensory-specific'brain regions, neural responses, and judgments. Neuron 57, 11–23.
Durand, A.C., Gould, G.M., 1910. A method of determining ocular dominance. J. Am. Med. Assoc. 55, 369–370.
Eickhoff, S.B., Stephan, K.E., Mohlberg, H., Grefkes, C., Fink, G.R., Amunts, K., Zilles, K., 2005. A new SPM toolbox for combining probabilistic cytoarchitectonic maps and functional imaging data. NeuroImage 25, 1325–1335.
Eickhoff, S.B., Paus, T., Caspers, S., Grosbras, M.H., Evans, A.C., Zilles, K., Amunts, K., 2007. Assignment of functional activations to probabilistic cytoarchitectonic areas revisited. NeuroImage 36, 511–521.
Frazier, J.A., Chiu, S., Breeze, J.L., Makris, N., Lange, N., Kennedy, D.N., Herbert, M.R., Bent, E.K., Koneru, V.K., Dieterich, M.E., Hodge, S.M., Rauch, S.L., Grant, P.E., Cohen, B.M., Seidman, L.J., Caviness, V.S., Biederman, J., 2005. Structural brain magnetic resonance imaging of limbic and thalamic volumes in pediatric bipolar disorder. Am. J. Psychiatr. 162, 1256–1265.
Goldstein, J.M., Seidman, L.J., Makris, N., Ahern, T., O'Brien, L.M., Caviness Jr., V.S., Kennedy, D.N., Faraone, S.V., Tsuang, M.T., 2007. Hypothalamic abnormalities in schizophrenia: sex effects and genetic vulnerability. Biol. Psychiatry 61, 935–945.
Hoover, A.E.N., Harris, L.R., Steeves, J.K.E., 2012. Sensory compensation in sound

localization in people with one eye. Exp. Brain Res. 216, 565–574.
Hutsler, J., Galuske, R.A., 2003. Hemispheric asymmetries in cerebral cortical networks. Trends Neurosci. 26, 429–435.
Jenkinson, M., Smith, S., 2001. A global optimisation method for robust affine registration of brain images. Med. Image Anal. 5, 143–156.
Jenkinson, M., Bannister, P., Brady, M., Smith, S., 2002. Improved optimization for the robust and accurate linear registration and motion correction of brain images. NeuroImage 17, 825–841.
Jones, D.K., 2008. Studying connections in the living human brain with diffusion MRI. Cortex 44, 936–952.
Jones, D.K., Knösche, T.R., Turner, R., 2013. White matter integrity, fiber count, and other fallacies: the do's and don'ts of diffusion MRI. NeuroImage 73, 239–254.
Kelly, K.R., Moro, S.S., Steeves, J.K.E., 2012. Living with one eye: plasticity in visual and auditory systems. In: Steeves, J.K.E., Harris, L.R. (Eds.), Plasticity in Sensory Systems. Cambridge University Press, Cambridge, UK, pp. 94–108.
Kelly, K.R., McKetton, L., Schneider, K.A., Gallie, B.L., Steeves, J.K.E., 2014. Altered anterior visual system development following early monocular enucleation. NeuroImage Clin. 4, 72–81.
Kelly, K.R., DeSimone, K.D., Gallie, B.L., Steeves, J.K.E., 2015. Increased cortical surface area and gyrification following long-term survival from early monocular enucleation. NeuroImage Clin. 7, 297–305.
Le Bihan, D., 2003. Looking into the functional architecture of the brain with diffusion MRI. Nat. Rev. Neurosci. 4, 469–480.
Li, J., Lam, C.S.Y., Yu, M., Hess, R.F., Chan, L.Y.L., Maehara, G., Woo, G.C., Thompson, B., 2010. Quantifying sensory eye dominance in the normal visual system: a new technique and insights into variation across traditional tests. Invest. Opthalmol. Vision Sci. 51, 6875–6881.
Martuzzi, R., Murray, M.M., Michel, C.M., Thiran, J.P., Maeder, P.P., Clarke, S., Meuli, R.A., 2007. Multisensory interactions within human primary cortices revealed by BOLD dynamics. Cerbral Cortex 17, 1672–1679.
Menon, R.S., Ogawa, S., Strupp, J.P., Uğurbil, K., 1997. Ocular dominance in human V1 demonstrated by functional magnetic resonance imaging. J. Neurophysiol. 77, 2780–2787.
Merabet, L.B., Pascual-Leone, A., 2010. Neural reorganization following sensory loss: the opportunity of change. Nat. Rev. Neurosci. 11, 44–52.
Meyer, K., Kaplan, J.T., Essex, R., Webber, C., Damasio, H., Damasio, A., 2010. Predicting visual stimuli on the basis of activity in auditory cortices. Nat. Neurosci. 13, 667.
Miki, A., Liu, G.T., Englander, S.A., van Erp, T.G., Bonhomme, G.R., Aleman, D.O., Haselgrove, J.C., 2001. Functional magnetic resonance imaging of eye dominance at 4 tesla. Ophthalmic Res. 33, 276–282.
Moro, S.S., Steeves, J.K.E., 2012. No Colavita effect: equal auditory and visual processing in people with one eye. Exp. Brain Res. 216, 267–373.
Moro, S.S., Steeves, J.K.E., 2013. No Colavita effect: increasing temporal load maintains equal auditory and visual processing in people with one eye. Neurosci. Lett. 556, 186–190.
Moro, S.S., Harris, L.R., Steeves, J.K.E., 2014. Optimal audiovisual processing in people with one eye. Multisens. Res. 27, 173–188.
Moro, S.S., Kelly, K.R., McKetton, L., Gallie, B.L., Steeves, J.K.E., 2015. Evidence of multisensory plasticity: asymmetrical medial geniculate body in people with one eye. NeuroImage Clin. 9, 513–518.
O'Brien, B.J., Olavarria, J.F., 1994. Anomalous patterns of callosal connections develop in visual cortex of monocularly enucleated hamsters. Biol. Res. 28, 211–218.
Olavarria, J., Malach, R., 1987. Development of visual callosal connections in neonatally enucleated rats. J. Comp. Neurol. 260, 321–348.
Pekkola, J., Ojanen, V., Autti, T., Jääskeläinen, I.P., Möttönen, R., Tarkiainen, A., Sams, M., 2005. Primary auditory cortex activation by visual speech: an fMRI study at 3T. Neuroreport 16, 125–128.
Pierpaoli, C., Basser, P.J., 1996. Toward a quantitative assessment of diffusion anisotropy. Magn. Reson. Med. 36, 893–906.
Röder, B., Stock, O., Bien, S., Neville, H., Rösler, F., 2002. Speech processing activates visual cortex in congenitally blind humans. Eur. J. Neurosci. 16, 930–936.
Rombouts, S.A., Barkhof, F., Sprenger, M., Valk, J., Scheltens, P., 1996. The functional basis of ocular dominance: functional MRI (fMRI) findings. Neurosci. Lett. 221, 1–4.
Schmierer, K., Wheeler-Kingshott, C.A., Boulby, P.A., Scaravilli, F., Altmann, D.R., Barker, G.J., Tofts, Paul S., Miller, D.H., 2007. Diffusion tensor imaging of post mortem multiple sclerosis brain. NeuroImage 35, 467–477.
Schroeder, C.E., Foxe, J., 2005. Multisensory contributions to low-level, 'unisensory' processing. Curr. Opin. Neurobiol. 15, 454–458.
Shu, N., Li, J., Li, K., Yu, C., Jiang, T., 2009. Abnormal diffusion of cerebral white matter in early blindness. Hum. Brain Mapp. 30, 220–227.
Smith, S.M., 2002. Fast robust automated brain extraction. Hum. Brain Mapp. 17, 143–155.
Smith, S.M., Jenkinson, M., Woolrich, M.W., Beckmann, C.F., Behrens, T.E., Johansen-Berg, H., Bannister, P.R., De Luca, M., Drobnjak, I., Flitney, D.E., Niazy, R.K., Saunders, J., Vickers, J., Zhang, Y., De Stefano, N., Brady, J.M., Matthews, P.M., 2004. Advances in functional and structural MR image analysis and implementation as FSL. NeuroImage 23, S208–S219.
Smith, S.M., Jenkinson, M., Johansen-Berg, H., Rueckert, D., Nichols, T.E., Mackay, C.E., Watkins, K.E., Ciccarelli, O., Cader, M.Z., Matthews, P.M., Behrens, T.E., 2006. Tract-based spatial statistics: voxelwise analysis of multi-subject diffusion data. NeuroImage 31, 1487–1505.
Song, S.K., Sun, S.W., Ramsbottom, M.J., Chang, C., Russell, J., Cross, A.H., 2002. Dysmyelination revealed through MRI as increased radial (but unchanged axial) diffusion of water. NeuroImage 17, 1429–1436.
Song, S.K., Yoshino, J., Le, T.Q., Lin, S.J., Sun, S.W., Cross, A.H., Armstrong, R.C., 2005. Demyelination increases radial diffusivity in corpus callosum of mouse brain. NeuroImage 26, 132–140.
Steeves, J.K.E., González, E.G., Steinbach, M.J., 2008. Vision with one eye: a review of visual function following monocular enucleation. Spat. Vis. 21, 509–529.
Toosy, A.T., Werring, D.J., Plant, G.T., Bullmore, E.T., Miller, D.H., Thompson, A.J., 2001. Asymmetrical activation of human visual cortex demonstrated by functional MRI with monocular stimulation. NeuroImage 14, 632–641.
Weeks, R., Horwitz, B., Aziz-Sultan, A., Tian, B., Wessinger, C.M., Cohen, L.G., Hallett, M., Rauschecker, J.P., 2000. A positron emission tomographic study of auditory localization in the congenitally blind. J. Neurosci. 20, 2664–2672.
Wong, N.A., Rafique, S.A., Kelly, K.R., Moro, S.S., Gallie, B.L., Steeves, J.K.E., 2018. Altered white matter structure in the visual system following early monocular enucleation. Hum. Brain Mapp. 39, 133–144.
Yu, C., Shu, N., Li, J., Qin, W., Jiang, T., Li, K., 2007. Plasticity of the corticospinal tract in early blindness revealed by quantitative analysis of fractional anisotropy based on diffusion tensor tractography. NeuroImage 36, 411–417.
Zatorre, R.J., 1989. Perceptual asymmetry on the dichotic fused words test and cerebral speech lateralization determined by the carotid sodium amytal test. Neuropsychologia 27, 1207–1219.
Zatorre, R.J., Belin, P., Penhune, V.B., 2002. Structure and function of auditory cortex: music and speech. Trends Cogn. Sci. 6, 37–46.